

Evolution of the Fermi surface of arsenic through the rhombohedral to simple-cubic phase transition: a Wannier interpolation study

Patricia K. Silas,¹ Peter D. Haynes,² and Jonathan R. Yates³

¹*Theory of Condensed Matter, Cavendish Laboratory, University of Cambridge, JJ Thomson Avenue, Cambridge CB3 0HE, United Kingdom*

²*Departments of Materials and Physics, Imperial College London, Exhibition Road, London SW7 2AZ, United Kingdom*

³*Department of Materials, University of Oxford, Parks Road, Oxford OX1 3PH, United Kingdom*
(Dated: August 19, 2014)

The pressure dependence of the Fermi surface of arsenic is examined using the technique of Wannier interpolation, enabling a dense sampling of the Brillouin zone and the ability to capture fine features within it. Focusing primarily on the A7 \rightarrow simple-cubic phase transition, we find that this semimetal to metal transition is accompanied by the folding of Fermi surfaces. The pressure dependence of the density of states (DOS) of arsenic indicates that the onset of the Peierls-type cubic to rhombohedral distortion is signified by the appearance of emerging van Hove singularities in the DOS, especially around the Fermi level. As we noted in an earlier study, high levels of convergence are consequently required for an accurate description of this transition.

I. INTRODUCTION

At ambient pressures the group-V element arsenic is a semimetal with the rhombohedral α -As or A7 crystal structure (space group $R\bar{3}m$). Under applied pressure arsenic undergoes a series of structural phase transitions,¹ the first of which occurs at approximately 28 GPa yielding the metallic simple-cubic (sc) structure (space group $Pm\bar{3}m$). The change in the electronic structure of arsenic across this semimetal to metal phase transition is described most naturally using the Fermi surface. In the A7 phase, arsenic is known to have a very unusual Fermi surface, consisting of six lobes connected by six long thin cylinders or “necks”. This Fermi surface is today still depicted as it was by Lin and Falicov² in 1966—an artist’s rendition—it is a famous image that is often used to describe the complexity that a Fermi surface may exhibit. First-principles calculations on the very dense grids required to resolve the fine details of the Fermi surface of arsenic are computationally expensive even with contemporary computing resources. Here we demonstrate that the method of Wannier interpolation^{3–6} achieves the same accuracy far more inexpensively.

In this study we use Wannier interpolation to investigate the pressure dependence of the Fermi surface and density of states (DOS) of arsenic, in particular as it experiences the A7 \rightarrow sc semimetal to metal phase transition. Wannier interpolation of the band structure is based on the use of maximally-localized Wannier functions (MLWFs),^{7–9} which act in the spirit of “tight-binding” as a set of spatially-localized orbitals, allowing calculations to be performed with the accuracy of first principles simulations but at low computational cost. Indeed, arsenic provides us with a beautifully simple demonstration of the power of Wannier interpolation—it is an ideal testing ground for the use of this technique to study phase transitions involving a metal.

In an earlier work we used density-functional theory (DFT) to determine the transition pressure of the

A7 \rightarrow sc phase transition of arsenic.¹⁰ The investigation consisted of performing relaxations of the two-atom unit cell subjected to pressures over the range of 0–200 GPa. The study was focused primarily on the A7 \rightarrow sc semimetal to metal phase transition. That work enabled us to address a long-standing question as to whether experimental results for the transition pressure obtained by Beister, *et al.*¹¹ were correct over those of Kikegawa and Iwasaki,¹² with our results supporting the findings of the former. It further allowed us to explain the wide range of theoretical values for the transition pressure that can be found in the literature—the spread of values is due to the difficulty of adequately sampling the Brillouin zone (BZ). We discovered that high-quality results required extensive convergence testing with respect to BZ sampling and amount of smearing used. In particular, we found that in order to ensure convergence and reliability of results when studying phase transitions involving a metal, dense BZ sampling grids are essential.¹³

We thus begin by using Wannier interpolation to determine the Fermi surface of arsenic at 0 GPa. We inspect closely the finest features of the electron and hole Fermi surfaces at ambient pressures and make a quantitative comparison of our results with those available in the literature. Building on the results obtained from the relaxations performed in our earlier study,¹⁰ we then use Wannier interpolation to investigate the pressure dependence of the Fermi surface of arsenic, and in particular to study exactly how it evolves through the A7 \rightarrow sc transition. Finally, we use Wannier interpolation to investigate the DOS of arsenic over a range of different pressures. In our earlier study, we found that converging our geometry optimizations in the vicinity of the A7 \rightarrow sc phase transition was rather more difficult than expected.^{10,13} We will see that this is due to the rapid change of the DOS around the Fermi level across the transition. Consequently, high levels of convergence are required in order to calculate the transition pressure accurately.

The paper is organized as follows. Section II outlines important technical aspects of the methodology, and Sec. III deals with the computational details of our calculations. In Secs. IV–VII, we present and discuss our results: we reveal the actual Fermi surface of uncompressed arsenic—the features thereof are compared to results of theory and experiment that exist in the literature; we study the pressure dependence of the Fermi surface of arsenic, with a view to observing it as it undergoes the A7 \rightarrow sc structural phase transition; we calculate the Wannier-interpolated DOS of arsenic in the A7 and sc phases, and we present the pressure dependence of the DOS of arsenic in the immediate vicinity of the A7 \rightarrow sc transition; we conclude with a brief discussion.

II. METHODOLOGY

A. Wannier Interpolation

A conventional electronic-structure calculation yields a set of Bloch states describing the low-lying band structure of a particular system in its ground state. A set of (generalized) Wannier functions¹⁴ (WFs) can be constructed from these Bloch states in order to be able to describe the system in real space, with the WFs acting as a basis set of localized orbitals. The method of Wannier interpolation^{3–6} is based on the use of a *unique* set of Wannier functions, the so-called “maximally-localized Wannier functions”,^{7–9} which serve as an “exact tight-binding” basis for the target system. Prescriptions due to Marzari and Vanderbilt⁷ and Souza, Marzari and Vanderbilt⁸ allow the determination of this unique set of Wannier functions—the former in the case of a set of isolated bands and the latter extended to the case of a set of entangled bands—by requiring the resulting WFs to exhibit minimum spread.

Wannier interpolation is a simple and widely applicable scheme that incorporates the idea of a tight-binding model with the accuracy of *ab initio* methods. The technique is ideal for the evaluation of quantities that require a very dense sampling of the BZ. In particular, it should be very useful for the study of metallic systems as it enables a sampling of the Fermi surface to *ab initio* accuracy but with little associated cost.

Here we are concerned with finding the eigenvalues of the one-electron effective Hamiltonian at arbitrary \mathbf{k} , $\varepsilon_{n\mathbf{k}}$, where n is the band index. However, this interpolation procedure can be extended to the calculation of other quantities of interest—the eigenvalues of any periodic one-electron operator can be determined in a similar fashion.³

B. Adaptive Smearing

To accelerate the convergence of singularities in the DOS, we apply a state-dependent broadening scheme as follows. Within the Wannier interpolation method, we

have the ability to vary the smearing of the occupancies according to the band gradients $|\partial\varepsilon_{n\mathbf{k}}/\partial\mathbf{k}|$, as the gradients can be computed efficiently at no additional cost. The state-dependent smearing width $W_{n\mathbf{k}}$ is set to³

$$W_{n\mathbf{k}} = a \left| \frac{\partial\varepsilon_{n\mathbf{k}}}{\partial\mathbf{k}} \right| \Delta k, \quad (1)$$

where a is a dimensionless constant, of value 0.2 in this study. This state-dependent broadening scheme is termed “adaptive smearing”³ and it enables highly resolved DOSs, especially when combined with the method of cold smearing.¹⁵

III. COMPUTATIONAL DETAILS

We build on the findings of our earlier studies of arsenic,¹⁰ in which structural relaxations were performed on the two-atom rhombohedral unit cell subjected to a range of pressures. These geometry optimizations resulted in a series of pressure-dependent configurations, characterized by the lattice parameters which are described in the discussion of the unit cell of arsenic found in the material supplementary to this study.¹⁶ For each configuration (each pressure), we repeat exactly the same procedure.

The computational details are as follows. For each pressure investigated, we first obtain the Bloch states self-consistently using the density-functional-based PWSCF code¹⁷ in the local-density approximation (LDA). We use a scalar-relativistic, norm-conserving pseudopotential generated using the “atomic” code (by A. Dal Corso, supplied with the Quantum Espresso distribution¹⁷) to describe the core-valence interaction of arsenic. The pseudopotential core radii are as follows: 1.16 Å for the 4s and 4p states, and 1.22 Å for the 4d states, anticipating that we will need to allow for *d*-states at higher pressures.

We perform the self-consistent calculation on our two-atom unit cell of arsenic using a 25×25×25 Monkhorst-Pack grid, which includes the Γ point. A kinetic energy cutoff of 750 eV is used for the plane-wave expansion of the valence wavefunctions. A convergence threshold of 1.4×10^{-8} eV is set for the minimization of the total energy, and a cold smearing¹⁵ of 0.27 eV is used.

Once the ground state charge density of the system has been determined, using the PWSCF code we then perform a non-self-consistent calculation in order to obtain a reference (*ab initio*) band structure against which the Wannier-interpolated band structure can be compared.

To calculate the WFs, the self-consistent potential is frozen and a non-self-consistent calculation is performed in order to discretize the Bloch states over a uniform mesh of 8×8×8 \mathbf{q} -points. The strong localization of the MLWFs in real space, in addition to the generally-accepted exponential fall-off of the WFs, ensures that a grid of this size is sufficient for our needs.³ (In this

work we adopt the convention used in Ref. 3 of using the symbol \mathbf{q} to denote grid points that belong to the mesh upon which the Bloch states have been stored. This is in order to distinguish these specific \mathbf{q} -points from arbitrary sites, labeled \mathbf{k} -points, at which the values are obtained through interpolation.) The Bloch states are thus stored on a relatively coarse *ab initio* grid. We have determined that we must use 9 WFs per atom of the unit cell in order to ensure that we can capture the character of the bands at higher pressures—this point is elaborated upon in the supplementary material.¹⁶ Thus we must construct 18 WFs and with this in mind, we calculate the first 30 bands at each \mathbf{q} -point. The 18 WFs can then be constructed from these 30 bands according to the disentanglement procedure prescribed by Souza, Marzari and Vanderbilt.⁸ This is performed using the WANNIER90 code.¹⁸

We obtain highly converged DOSs across the range of pressures studied using a $400 \times 400 \times 400$ interpolation (\mathbf{k} -point) mesh.

Although we use the PWSCF code in the LDA, the configurations (the lattice parameters defining the structure of arsenic at each pressure) used in this study were obtained from calculations using the Perdew-Burke-Ernzerhof generalized gradient approximation¹⁹ (abbreviated here as GGA-PBE) for the exchange-correlation functional.¹⁰ We have confirmed that when using Wannier interpolation to study the GGA-PBE configurations, it makes no significant difference whether the ground state potential has been set up using an LDA functional or a GGA functional.

IV. THE FERMI SURFACE OF ARSENIC

At 0 GPa, when it is in the A7 phase, arsenic is a semimetal. Only the fifth and sixth bands cross the Fermi level giving rise to the hole and electron Fermi surfaces, respectively. The BZ of the primitive rhombohedral (A7) structure of arsenic is presented in Fig. 1. This figure was taken from Ref. 20, though it was originally published by M. H. Cohen in 1961,²¹ and it is the same for arsenic as it is for the other group-V semimetals, antimony and bismuth. The special points of the rhombohedral BZ indicated in Fig. 1 have been written out explicitly by Falicov and Golin,²² and are given in the supplementary material that accompanies this work.¹⁶

The hole Fermi surface, or hole “crown”, of arsenic depicted in Fig. 2 was determined by Lin and Falicov via an empirically-based pseudopotential band structure calculation in 1966.² It is an artist’s rendition, and it is still used today to illustrate the Fermi surface of arsenic.

We use Wannier interpolation to calculate the Fermi surface of arsenic (at 0 GPa) for the first time since Lin and Falicov’s calculation. From our $8 \times 8 \times 8$ *ab initio* grid, we interpolate onto a $150 \times 150 \times 150$ \mathbf{k} -point grid spanning the BZ in an effort to capture the finest details of the Fermi surface. Given the results of this interpolation and

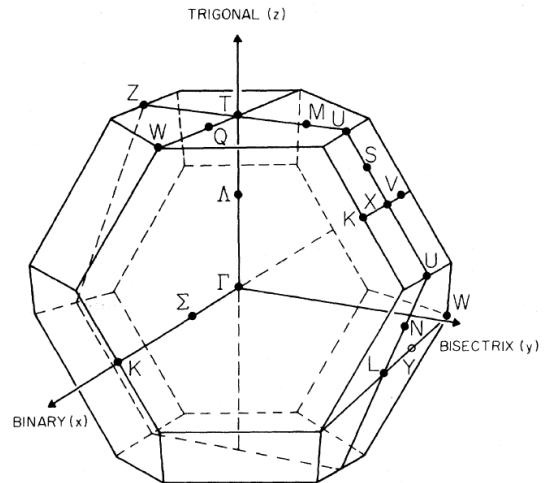


FIG. 1: The BZ of the primitive rhombohedral (A7) structure, labeled with points and lines of symmetry^{21,22} and with the mutually orthogonal binary (x), bisectrix (y) and trigonal (z) axes. This figure is taken from Ref. 20. The point along the TW line close to T is labeled as Q in this figure—this point is usually called “B” in the literature and we refer to it throughout this work as B. The special points appearing in the figure are defined explicitly in the supplementary material.¹⁶

the Fermi energy computed in the initial self-consistent calculation, the Fermi surface is plotted.

The hole Fermi surface of arsenic at 0 GPa resulting from our Wannier interpolation is depicted in Fig. 3—this is as it appears in the reciprocal unit cell. This Fermi surface does closely resemble Lin and Falicov’s hole crown. We will investigate how closely further below.

The hole Fermi surface, centered at the point T, is composed of six lobe-like pockets connected by six long thin cylinders or necks, each of which is due to a point “B” of accidental degeneracy located along the TW line and only slightly above the Fermi level. (This accidental degeneracy is believed to be lifted when the spin-orbit coupling is taken into account.^{2,24}) The lobes are each bisected by a plane containing the trigonal (ΓT) and bisectrix (ΓU) axes (by a mirror plane). The maximum of the fifth band occurs within the lobe and on the mirror plane at a point designated as “H”.

The electron Fermi surface is composed of three ellipsoid-like pockets centered at each of the three equivalent L points of the BZ (minimum of the sixth band occurring at L). The merged hole and electron Fermi surfaces of arsenic at 0 GPa are shown in Fig. 4, where the binary (TW) axis lies along the horizontal and the bisectrix (TU) axis lies along the vertical (see Figs. 1 and 2).

We will now go into more detail by looking at certain cross sections of interest of the hole and electron Fermi surfaces of arsenic at 0 GPa, and by comparing our results with those that are available in the literature. This will require interpolating onto two-dimensional grids—slices through the BZ. The Fermi contours resulting from

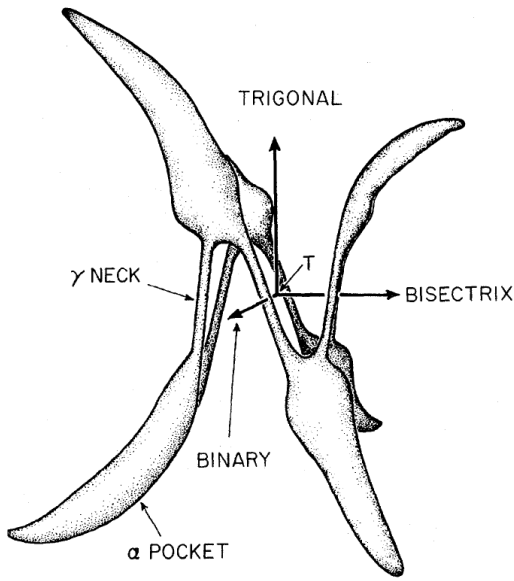


FIG. 2: Lin and Falicov's² hole crown, taken from Ref. 20. The hole Fermi surface is centered at T. The mutually orthogonal binary (x), bisectrix (y) and trigonal (z) axes are included.

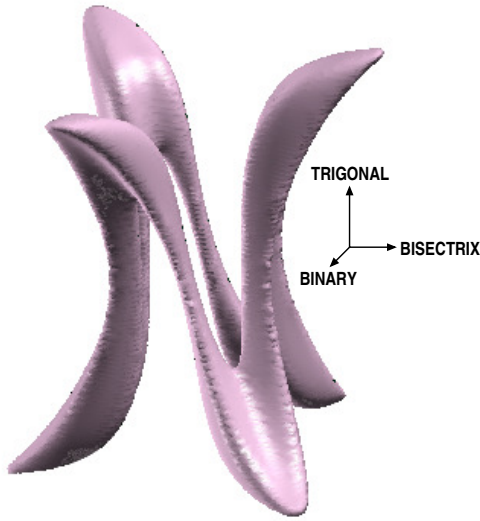


FIG. 3: (Color online) The hole crown of arsenic at 0 GPa as it appears in the reciprocal unit cell. The mutually orthogonal binary, bisectrix and trigonal axes are included. This has been plotted using the XCRYSDEN package.²³

the intersection of these slices with the Fermi surface are subsequently plotted and examined.

We reveal next the intersection of one of these slices through the BZ with the hole Fermi surface, resulting in the contour displayed in Fig. 5. Here we have sliced the hole Fermi surface parallel to the trigonal-bisectrix plane and passing through B. We include as an inset of this figure the equivalent contour obtained by Lin and Falicov in 1966.² Our Fermi contour is considerably more detailed than that of Lin and Falicov. The contours resulting

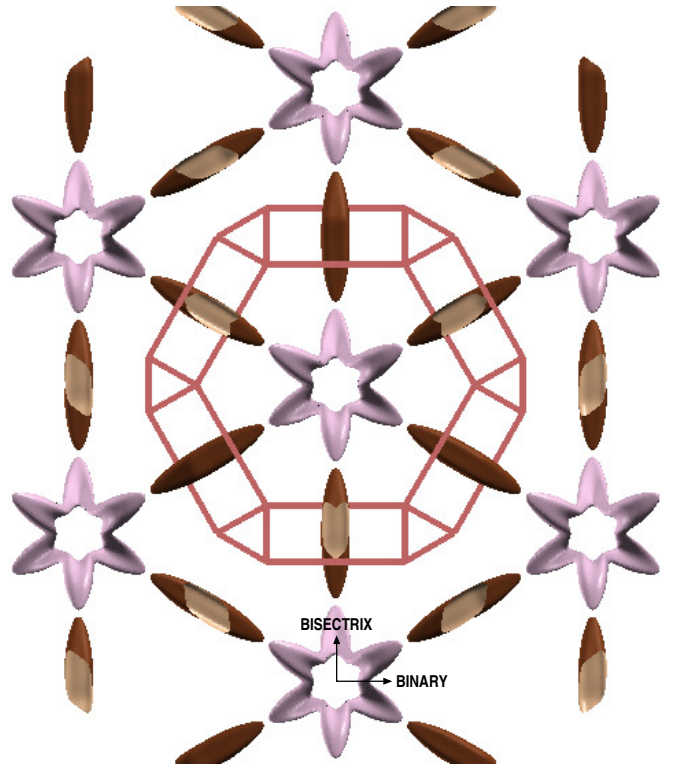


FIG. 4: (Color online) The uncropped hole and electron Fermi surfaces of arsenic at 0 GPa, where the first BZ is displayed. The hole Fermi surface (in light gray/pink) is centered at the point T. Three of the six lobes shown are up, three down. The electron Fermi surface (in dark gray/brown) is comprised of three ellipsoid-like pockets centered at the three equivalent L points of the BZ. The bisectrix axis (TU) is along the vertical, the binary axis (TW) along the horizontal. The trigonal axis is through the origin and out of the page.

from the other slices we inspected are presented in the supplementary material,¹⁶ but all results are summarized in Table I and contrasted against any data previously published in the literature.

V. PRESSURE DEPENDENCE OF THE FERMI SURFACE OF ARSENIC: THE A7 \rightarrow SC PHASE TRANSITION

We illustrate in Fig. 6 the evolution of the electron and hole Fermi surfaces⁴⁸ of arsenic as it undergoes the A7 \rightarrow sc phase transition. This figure is complemented by the corresponding Animations 01–03,^{31–33} of the supplementary material provided.¹⁶ These animations show the phase transition happening over a finer resolution of pressures than is shown in Fig. 6, and thus give a better idea of what happens to the Fermi surface through the transition.

Fig. 6 consists of three columns, each representing a different cross section of the BZ. The four rows of the figure refer to four different pressures: 0 GPa, 10 GPa, 20 GPa and 35 GPa. In all three columns, the bisectrix

TABLE I: Features of the electron and hole Fermi surfaces of arsenic.

Electron Fermi surface. All areas are in \AA^{-2}	Ref. 2 (Theory)	Ref. 25 (Experiment)	Ref. 20 (Experiment)	This work ^a
Area normal to the binary [see Fig. S3 ^b]: trigonal-bisectrix plane through L	0.0571 ^c	0.0732 ± 0.0002	0.0733	0.088
Tilt angle ^d	-8°	$-9.0 \pm 0.2^\circ$		-10.6°
Area normal to the trigonal [see Fig. S4]: binary-bisectrix plane through L	0.0643	0.0746 ± 0.0002	0.0746	0.096
Area normal to the bisectrix [see Fig. S5]: trigonal-binary plane through L			0.0202	0.026
Hole Fermi surface. All areas are in \AA^{-2}				
Area normal to the binary [see Fig. S6]: trigonal-bisectrix plane through Γ	0.0343	0.01422 ± 0.00002	0.0275	0.027
Tilt angle	$\sim +44^\circ$	$+37.25 \pm 0.1^\circ$	$+37.3 \pm 1.5^\circ$	$+37.8^\circ$
Area normal to the trigonal [see Fig. S7]: binary-bisectrix plane through T	$(2.464 \times 10^{-4})^e$	$(2.453 \pm 0.007) \times 10^{-4}$	0.0179	2.1×10^{-3}
Tilt of necks [see Fig. 5]	-11°	$-9.6 \pm 0.1^\circ$		$\sim -9.7^\circ$
Combined area normal to the bisectrix [see Fig. S8]: trig.-bin. plane through T			0.0367	0.030
Special \mathbf{k} -points H and B. Coordinates are fractional w.r.t. reciprocal lattice vectors.	Ref. 2	This work		
1 of 6 equivalent H points—maximum of the 5 th band (occurs in mirror plane)	[0.2043, 0.3758, 0.2043]	[0.2050, 0.3753, 0.2050]		
1 of 6 equivalent B points—point of accidental degeneracy along TW line	[0.4617, 0.5, 0.5383]	[0.4472, 0.4999, 0.5528]		

^a These values have been obtained using a Fermi energy recomputed from the Wannier-interpolated DOS of A7 arsenic at 0 GPa, presented in Sec. SV.

^b Figures for which the numbering begins with an “S” are found in the supplementary material provided.

^c Electron pockets: Fermi energy fixed so as to fit the minimum area for magnetic fields in the trigonal-bisectrix plane.

^d Angle convention followed throughout is that of Ref. 20 (see also Refs. 24–27): angles are measured in the trigonal-bisectrix plane or some parallel plane and with respect to the vertical—the trigonal axis (ΓT) or some parallel line. Positive rotations are in the sense from ΓT to ΓX in the first quadrant of the coordinate system.

^e Hole pockets: Fermi energy fixed so as to fit this area.

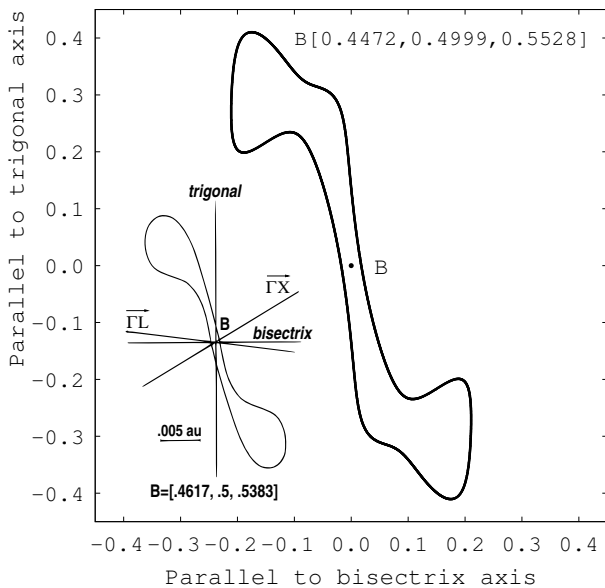


FIG. 5: Hole pocket: trigonal-bisectrix plane through B. This figure has been obtained using a Fermi energy recomputed from the Wannier-interpolated DOS of A7 arsenic at 0 GPa, presented in Sec. SV. All distances are in \AA^{-1} . The inset is the analogous cross section as calculated by Lin and Falicov.²

axis lies along the horizontal. For the left-hand column the trigonal axis lies along the vertical, whereas for the other two columns the binary axis lies along the vertical. Arsenic is in the A7 phase for the first three rows—it is in the sc phase in the fourth row. Hole surface contours are in black and electron surface contours are in gray (green).

This investigation complements our earlier studies of the A7 \rightarrow sc phase transition of arsenic.¹⁰ The configurations resulting from geometry optimizations performed on arsenic subjected to pressures up to 200 GPa in that work act as the starting point here for our studies of ar-

senic using Wannier interpolation. We present our findings concerning the higher-pressure phase transitions of arsenic in the supplementary material provided.¹⁶ We expect the A7 \rightarrow sc phase transition to occur at 28 ± 1 GPa.

We first discuss the left-hand column of Fig. 6, in which the A7 \rightarrow sc phase transition is most noticeable. The left-hand column of Fig. 6 corresponds to the intersection of the BZ with the trigonal-bisectrix plane through Γ (it is a mirror plane and contains the points Γ , T, L, X and U as indicated in the figure). The trigonal axis is the finely dotted vertical line. The other two lines in the diagrams on the left serve to compare orientations with the other two columns.

As we scan from top to bottom in this first column (corresponding to Animation 01³¹), we see that the hole surface initially centered on T distorts in such a way that by the bottom panel there is a folded cubic surface (cut along the body diagonal) centered at Γ . Arsenic at 35 GPa is in the sc phase. The surface is folded due to the fact that we have two atoms in the unit cell. We notice too that by 10 GPa an electron pocket has opened up at T (it has actually already opened up by 8 GPa). Our Fermi surfaces fold from about 27 GPa, agreeing with our expected transition pressure of 28 ± 1 GPa.

For the middle column of Fig. 6 (corresponding to Animation 02³²), the BZ has been sliced by the binary-bisectrix plane through T. This slice thus also contains points W and U as indicated. The dotted-dashed line in these figures is the bisectrix axis—as a visual aid for orientation purposes, the bisectrix axis can be compared for corresponding panels of the left-hand and middle columns. The phase transition, again from about 27 GPa, seems to happen when the hole pockets that have opened up at W are just touching the electron pockets appearing on either side of them.

In the right-hand column of Fig. 6 (corresponding to Animation 03³³), the BZ has been sliced by the binary-bisectrix plane through Γ . The dashed lines appearing in the panels of this column correspond to the dashed lines

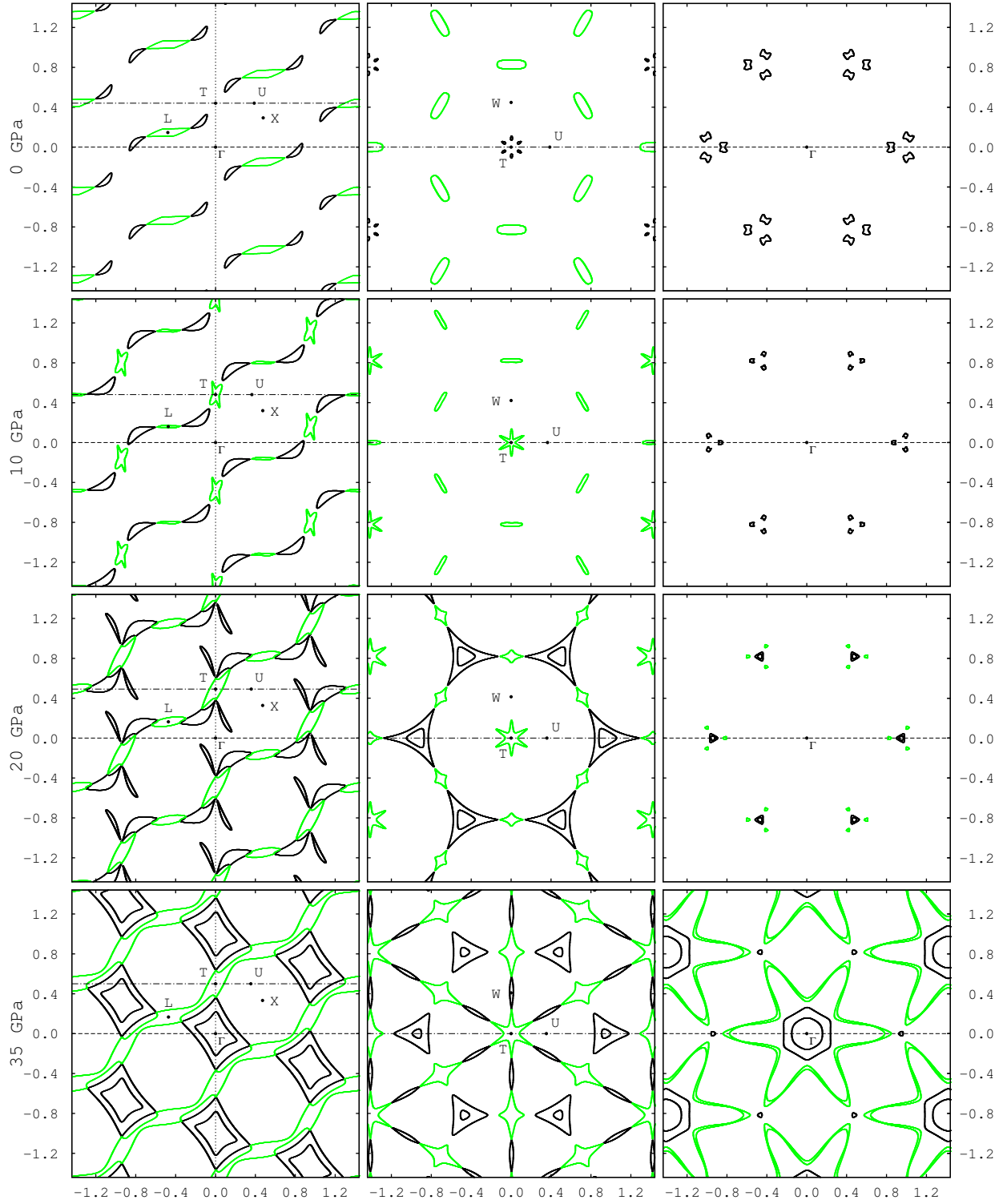


FIG. 6: (Color online) Pressure dependence of the Fermi surface of arsenic: 0–35GPa. For the left-hand column, the BZ has been intersected by the trigonal-bisectrix plane; the middle column by the binary-bisectrix plane through T; the right-hand column by the binary-bisectrix plane through Γ . The bisectrix axis (the dotted-dashed line) is along the horizontal for all three columns. The trigonal axis (the finely dotted line) is along the vertical for the left-hand column. The binary axis is along the vertical for the middle and right-hand columns. All distances are fractional with respect to the length of the reciprocal lattice vector—this is to enable comparisons across pressures. Hole contours are in black, electron contours in gray (green). The cross section of the hole crown centered at T can be seen in the top left panel. The A7 \rightarrow sc phase transition takes place at a pressure between those represented in the bottom two rows of the figure. In the bottom row (at 35 GPa) arsenic is simple cubic—the use of a two-atom unit cell causes the folding evidenced especially in the bottom left and bottom right panels.

appearing in the panels of the left-hand column of the figure. At about 27 GPa, we once again see the folding of the individual electron and hole Fermi surfaces indicating that arsenic is now in the sc phase.

We have mentioned that the folding of the Fermi surfaces seen in the bottom row of Fig. 6 is due to the fact that we are using the two-atom unit cell to model arsenic over the entire range of pressures studied, whereas in the sc phase the primitive cell contains one atom. The *unfolded* Fermi surfaces can be inspected by comparing the bottom row of Fig. 6 with Fig. S9 of the supplementary material,¹⁶ in which are presented the corresponding results for sc arsenic at 35 GPa using a one-atom primitive cell. The BZ for the one-atom primitive sc structure can be found for example in Ref. 28 or more recently in Ref. 29.

Determining the pressure at which the A7 \rightarrow sc transformation of arsenic happens is difficult due to the nature of this semimetal to metal phase transition, which in our earlier study we found to be of second order.¹⁰ In that work, we investigated the pressure dependence of the lattice parameters of arsenic, and we determined the transition pressure according to when the internal coordinates had reached their high-symmetry values. However as the internal coordinates reached their high-symmetry values at two different pressures, there was still some question as to when the transition actually happens. Using Wannier interpolation we have observed the evolution of certain cross sections of interest of the Fermi surfaces across the transition. Wannier interpolation allows us to say that the folding of the Fermi surfaces is perhaps the best indication of when the A7 \rightarrow sc phase transition has occurred.

VI. WANNIER-INTERPOLATED DENSITIES OF STATES OF A7 AND SC ARSENIC

Wannier-interpolated DOSs for arsenic in the A7 phase at 0 GPa and in the sc phase at 35 GPa obtained using the WANNIER90 code¹⁸ are presented in Fig. 7. This figure can be compared with that which appears in Ref. 30. Our results agree at least qualitatively with those (the pressures corresponding to the DOSs in that publication are not specified), the only other DOS calculations of arsenic of which we are aware. It is evident that Wannier interpolation combined with adaptive smearing enables highly-accurate DOSs, allowing even the very finest of features to be captured. As we would expect, there is a dramatic increase in the DOS at the Fermi level as the pressure is increased through the A7 \rightarrow sc phase transition, during which arsenic changes from a semimetal to a metal. We have used our DOS calculations to recompute the Fermi energy of A7 arsenic at 0 GPa. We obtain a value that is 0.01 eV higher than that resulting from our self-consistent calculation using the PWSCF code, moving the Fermi level toward the minimum in the DOS that appears nearby.

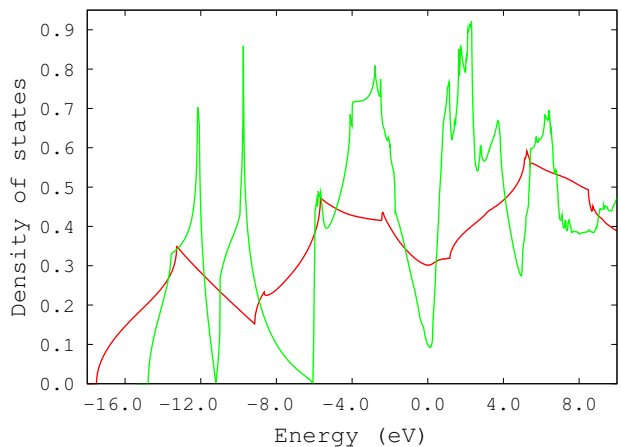


FIG. 7: (Color online) Wannier interpolation combined with adaptive smearing³ using cold smearing:¹⁵ comparing the DOSs of A7 and sc arsenic—the pressures are 0 GPa (gray/green) and 35 GPa (black/red), respectively. The DOSs are referenced to the Fermi level in both cases. This figure can be compared to that which appears in Ref. 30. Our results agree qualitatively with those. It is evident that Wannier interpolation combined with adaptive smearing enables features of the DOS to be captured on the very finest of scales. The DOS at the Fermi level can be seen to increase appreciably through the A7 \rightarrow sc transition, as arsenic changes from a semimetal to a metal.

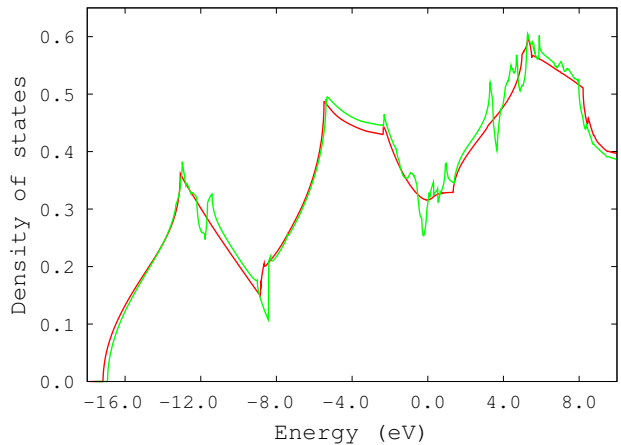


FIG. 8: (Color online) Evolution of the DOS of arsenic across the sc \rightarrow A7 phase transition. The DOSs of arsenic at 29 GPa (black/red) and at 25 GPa (gray/green) are referenced to the Fermi level and superimposed. It can be seen that as the pressure is lowered, the onset of the Peierls-type cubic to rhombohedral distortion is signified by the emergence of van Hove singularities in the DOS.

Next we inspect the evolution of the DOS of arsenic in the immediate vicinity of the A7 \rightarrow sc transition, and present our results in Fig. 8. In this figure, the DOSs for arsenic at 29 GPa and 25 GPa are referenced to the Fermi level and superimposed. Changes in the DOS are observed more clearly as the pressure is lowered such that

arsenic transitions from the higher-symmetry sc phase to the lower-symmetry A7 phase (the sc \rightarrow A7 transition). Thus we see from this figure that the onset of the Peierls-type cubic to rhombohedral distortion is signified by the emergence of van Hove singularities in the DOS, especially around the Fermi level. The rapidly changing DOS at the Fermi level explains why such high levels of convergence are required when studying this transition.¹⁰

In our earlier studies of arsenic,¹⁰ we had found that the rhombohedral angle α reaches its high-symmetry value at a lower pressure than does the atomic positional parameter z , and that the electronic change occurring as the pressure is increased through the A7 \rightarrow sc transition appeared to be driving the atomic positional parameter z to its high-symmetry value. A close inspection of the evolving DOS however, which can be seen in the supplementary material, reveals that the electronic change is instead driving α to its high-symmetry value.

VII. CONCLUSIONS

Wannier interpolation has enabled us to calculate the Fermi surface of arsenic at ambient pressures and through the A7 \rightarrow sc phase transition, obtaining first principles accuracy at vastly reduced computational cost. We found that the folding of the Fermi surfaces is perhaps the best indication of when the A7 \rightarrow sc phase transition has occurred. We further determined from our studies of the Wannier-interpolated DOS of arsenic over the range of pressures in the vicinity of the A7 \rightarrow sc phase transition, that the onset of the Peierls-type cubic to rhombohedral distortion is signified by the appearance of emerging van Hove singularities in the DOS especially around the Fermi level. The rapidly changing DOS at the Fermi level explains why such high levels of convergence are required when studying this transition, as we had found in our earlier studies of arsenic.¹⁰

Arsenic provides us with an example of a challenging system that is ideally suited to demonstrating the power of the Wannier interpolation technique. This methodology furthermore enables a novel approach to the study of semimetal to metal phase transitions, such as the A7 \rightarrow sc transition of arsenic, or in fact of any phase transitions involving a metal. The technique is a particularly valuable one for the accurate determination of Fermi surfaces, as well as for the calculation of highly resolved DOSs.

VIII. ACKNOWLEDGMENTS

We thank Richard Needs for helpful discussions. Computing resources were provided by the University of Cambridge High Performance Computing Service (HPCS). P.D.H. and J.R.Y. acknowledge the support of Royal Society University Research Fellowships.

Appendix: Evolution of the Fermi surface of arsenic through the rhombohedral to simple-cubic phase transition: a Wannier interpolation study—supplementary information

We review the Brillouin zone (BZ) corresponding to the two-atom primitive cell of rhombohedral (A7) arsenic, defining explicitly the special \mathbf{k} -points involved. This is followed by a discussion concerning the choice of the number of Wannier functions to construct in order to set up an “exact tight-binding” model at each given pressure from which Wannier interpolations can be performed. We elaborate on the features of the electron and hole Fermi surfaces of A7 arsenic at 0 GPa. We investigate the case of simple-cubic (sc) arsenic at 35 GPa using the one-atom primitive cell in order to inspect the “unfolded” Fermi surfaces, and to compare with the folded ones resulting from the use of the two-atom unit cell. We present the results of our studies of arsenic at pressures beyond which it is no longer in the sc phase, where once again the two-atom unit cell is employed. Finally, we elaborate on our studies of the density of states (DOS) of arsenic as it undergoes the A7 \rightarrow sc (space groups $R\bar{3}m \rightarrow Pm\bar{3}m$) phase transition, and present DOSs for A7, sc and body-centered-cubic (bcc) arsenic (space group $Im\bar{3}m$). These DOSs are contrasted against the band structures from which they originate.

Appendix SI: The Rhombohedral Brillouin Zone

The real-space primitive cell of A7 arsenic contains two atoms and is described by three lattice parameters: the length of the lattice vectors, a , the angle α between each pair of lattice vectors, and the atomic positional parameter z , where $z < 1/4$, which determines the fractional positions of the two atoms along the cell’s body diagonal. The BZ of the primitive rhombohedral structure—it is the same for each of the group-V semimetals: arsenic, antimony and bismuth—is presented in Fig. S1.⁴⁹ This figure was taken from Ref. 20, though it was originally published by M. H. Cohen in 1961.²¹ Cohen, Falicov and Golin²⁸ showed that much of the band structure of the group-V semimetals can be explained directly from their crystal structure.

The parameter ϵ as defined in Ref. 22 describes the shear that distorts the A7 structure from the sc structure. It is related to the rhombohedral angle α thus:

$$\epsilon = \frac{[1 - (1 + \cos \alpha - 2 \cos^2 \alpha)^{1/2}]}{\cos \alpha}. \quad (\text{A.1})$$

The structure of A7 arsenic can be pictured by imagining the interpenetration of two face-centered-cubic lattices (each one contributing an atom to the two-atom A7 primitive cell) offset from each other such that $z < 1/4$ and to which a shear has been applied in the [111] direction (along the trigonal axis), such that $\alpha < 60^\circ$. When

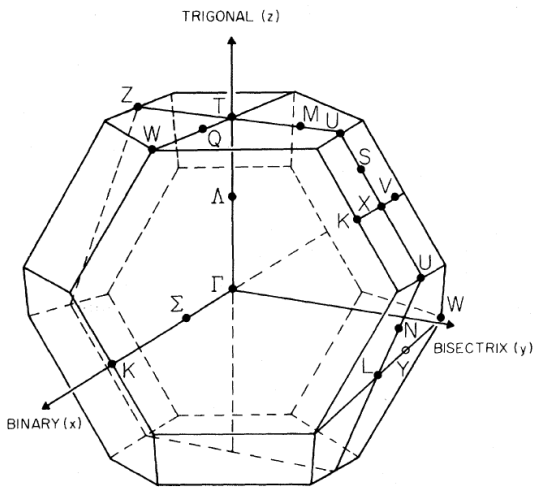


FIG. S1: The BZ of the primitive rhombohedral (A7) structure, labeled with points and lines of symmetry^{21,22} and with the mutually orthogonal binary (x), bisectrix (y) and trigonal (z) axes. This figure is taken from Ref. 20.

$\alpha = 60^\circ$, $\epsilon = 0$ and there is no shear—when both lattice parameters reach their high-symmetry values, $\alpha = 60^\circ$ and $z = 1/4$, the structure becomes simple cubic.

The special \mathbf{k} -points of the rhombohedral BZ indicated in Fig. S1 have been written out explicitly by Falicov and Golin,²² who follow Cohen’s notation for points and lines of symmetry.²¹ These points of symmetry are expressed in fractional coordinates (with respect to the reciprocal lattice vectors). Examples of each of these points are:

$$\Gamma = [0, 0, 0], \quad (\text{A.2})$$

$$X = [0, \frac{1}{2}, \frac{1}{2}], \quad (\text{A.3})$$

$$L = [0, \frac{1}{2}, 0], \quad (\text{A.4})$$

$$T = [\frac{1}{2}, \frac{1}{2}, \frac{1}{2}], \quad (\text{A.5})$$

$$W = [\gamma, 1 - \gamma, \frac{1}{2}], \quad (\text{A.6})$$

$$U = [\frac{1}{2}\gamma + \frac{1}{4}, 1 - \gamma, \frac{1}{2}\gamma + \frac{1}{4}], \quad (\text{A.7})$$

$$K = [0, \frac{3}{4} - \frac{1}{2}\gamma, \frac{1}{2}\gamma + \frac{1}{4}], \quad (\text{A.8})$$

where²²

$$\gamma = \frac{(1 + \frac{1}{2}\epsilon^2)}{(2 + \epsilon)^2}. \quad (\text{A.9})$$

Multiplicities and symmetry elements of these special \mathbf{k} -points can be found in Cohen.²¹ Other group theoretical considerations can be found in Falicov and Golin.²²

Note that the three special points W, U and K depend on γ , and thus on the rhombohedral angle α of the real-space primitive cell—their coordinates will therefore change as the pressure is increased. When $\alpha = 60^\circ$, $\epsilon = 0$ and $\gamma = \frac{1}{4}$. Thus in the two-atom representation of sc arsenic:

$$W_{\text{sc}} = [\frac{1}{4}, \frac{3}{4}, \frac{1}{2}], \quad (\text{A.10})$$

$$U_{\text{sc}} = [\frac{3}{8}, \frac{3}{4}, \frac{3}{8}], \quad (\text{A.11})$$

$$K_{\text{sc}} = [0, \frac{5}{8}, \frac{3}{8}]. \quad (\text{A.12})$$

As $\alpha \rightarrow 90^\circ$, $\epsilon \rightarrow -0.5$ and $\gamma = \frac{1}{2}$. Thus in the two-atom representation of bcc arsenic, the points W and U merge with T, and the point K merges with X:

$$W_{\text{bcc}} = U_{\text{bcc}} = T = [\frac{1}{2}, \frac{1}{2}, \frac{1}{2}], \quad (\text{A.13})$$

$$K_{\text{bcc}} = X = [0, \frac{1}{2}, \frac{1}{2}]. \quad (\text{A.14})$$

The convention is to label the three mutually orthogonal axes making up the coordinate system of the A7 BZ as follows. Referring again to Fig. S1, the binary axis is labeled the x -axis and contains the segment ΓK —it is parallel to the TW line. The bisectrix axis is labeled as the y -axis—it is parallel to the TU line but passes through Γ . The trigonal (z) axis passes through the segment ΓT . The trigonal and bisectrix axes define a mirror plane.

Angles measured in the BZ are reported according to a convention that is discussed in Refs. 24–27 and in Ref. 20. In the trigonal-bisectrix (mirror) plane, or some parallel plane, angles are measured with respect to the vertical (the trigonal axis, ΓT , or some parallel line). Positive rotations are in the sense from ΓT to ΓX in the first quadrant of the coordinate system. Our calculations of the unit cell of arsenic yield the following angles for the special points in the mirror plane: ΓT is at 0° , ΓX is at $+58.4^\circ$, ΓU is at $+41.3^\circ$ and ΓL is at -72.9° . These values are for the configuration resulting from a geometry optimization of A7 arsenic at 0 GPa (and 0 K) using the Perdew-Burke-Ernzerhof generalized gradient approximation¹⁹ (abbreviated in this work as GGA-PBE) for the exchange-correlation functional. The details of these calculations can be found in Ref. 10.

We will make some brief comparisons here and there between the two-atom and one-atom (primitive) cells of sc arsenic. The BZ for the one-atom primitive sc structure can be found for example in Ref. 28 or more recently in Ref. 29. Examples of the special points of this BZ are $\Gamma = [0, 0, 0]$, $R = [\frac{1}{2}, \frac{1}{2}, \frac{1}{2}]$, $M = [\frac{1}{2}, \frac{1}{2}, 0]$ and $X = [\frac{1}{2}, 0, 0]$. The BZ of the primitive sc structure is the “unfolded” version of the BZ of the two-atom unit cell in the sc configuration. In the two-atom BZ, the point R folds onto the point Γ , and the point M folds onto the point X.²⁸

Appendix SII: Choice of the Number of Wannier Functions to Construct

Initially, we began our studies using four Wannier functions per atom of the unit cell—the initial guesses for these were the hybrid sp^3 orbitals.¹⁸ However as is demonstrated in Fig. S2, in which the Wannier-interpolated bands (in green) have been obtained using four Wannier functions per atom of the unit cell, this choice turns out not to be well suited to studying arsenic at higher pressures. This is evidenced by the inability of the four Wannier functions to capture the states of the (red) *ab initio* band structure which can be seen to be descending (one of which in heavy black) toward the Fermi level with increasing pressure. In addition, in order for the band structure to be faithfully reproduced using only four Wannier functions at the higher pressures, we would be obliged to keep the “inner window” quite close to the Fermi level (see especially the bottom panel of Fig. S2, the band structure of arsenic at 200 GPa), yet we would like ideally to be able to place it a few eV above the Fermi level. (The inner window is the energy window within which the *ab initio* band structure is required to be preserved as per the disentanglement method of Souza, Marzari and Vanderbilt.⁸)

We choose therefore to address both points by working with nine Wannier functions per atom of the unit cell over the entire range of pressures studied. The trial functions used for the initial guesses of the nine Wannier functions are the six sp^3d^2 hybrid orbitals in addition to the d_{xy} , d_{yz} and d_{xz} orbitals,¹⁸ all atom-centered, and this turns out to be entirely satisfactory.

Appendix SIII: Further Details of the Electron and Hole Fermi Surfaces

1. Features of the Electron Fermi Surface

The electron Fermi surface of arsenic at 0 GPa is composed of three ellipsoid-like pockets centered at the three equivalent L points of the BZ. The intersection of the trigonal-bisectrix plane (the mirror plane) with an electron pocket at L results in the Fermi contour illustrated in Fig. S3. We have included as an inset of this figure the analogous cross section obtained by Lin and Falicov in 1966.²

Before we proceed, it is important to note that the Lin and Falicov calculations were based on experimental data (from de Haas-van Alphen experiments performed at temperatures between 1.2 and 4.2 K) available at the time—most of it available to them by private communication,² values which were later somewhat altered upon their publication.²⁵ Lin and Falicov fixed the Fermi energies of the electron and hole Fermi surfaces so as to fit the data available for certain features contained therein. In the case of the electron Fermi surface, the Fermi energy was adjusted to fit an area corresponding to the mini-

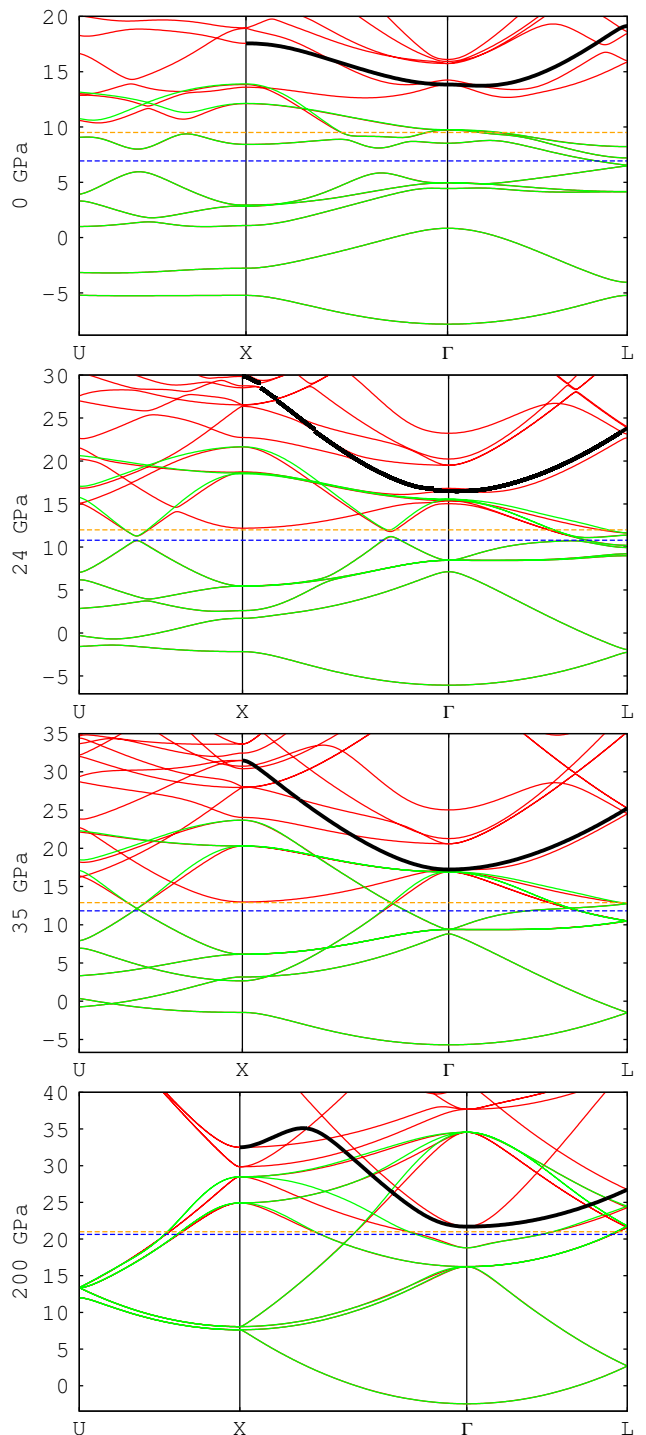


FIG. S2: Band structures of arsenic at 0, 24, 35 and 200 GPa (energy in eV). The Wannier-interpolated bands (in green) have been obtained using four Wannier functions per atom of the unit cell. The dotted blue line is the Fermi level and the dotted pink line indicates the top of the “inner window”. Arsenic is in the A7 phase at 0 and 24 GPa, in the sc phase at 35 GPa, and in the bcc phase at 200 GPa. Using four Wannier functions is not suitable for arsenic at higher pressures. As the pressure increases certain *ab initio* bands can be seen to be descending toward the Fermi level. One of these states is outlined in black—this state is not captured by the four sp^3 orbitals used as the initial guess for the Wannier functions.

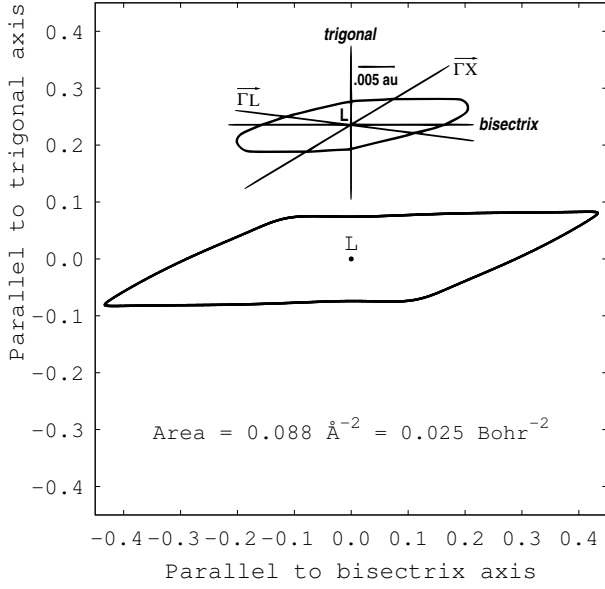


FIG. S3: Electron pocket: trigonal-bisectrix plane through L. This figure and the resulting area have been obtained using a Fermi energy recomputed from the Wannier-interpolated DOS of A7 arsenic at 0 GPa. All distances are in \AA^{-1} . This contour can be located in the top panel of the left-hand column of Fig. 6. The inset is the analogous cross section as calculated by Lin and Falicov.²

imum area observed for magnetic fields in the trigonal-bisectrix plane.^{2,25} In the case of the hole Fermi surface, the Fermi energy was adjusted to fit the area reported by Priestly, et al.²⁵ to correspond to a cross section of one of the long thin necks. Thus the calculations of Lin and Falicov have been adjusted to fit some prevalent experimental data. Nevertheless it is still edifying to compare our results with theirs.

Returning thus to Fig. S3, we see that the contour of our electron pocket in the trigonal-bisectrix plane is quite a bit sharper than that of Lin and Falicov. The area of this cross section, 0.088\AA^{-2} , is approximately 20% larger than that obtained from those early experiments, and it is approximately 55% larger than that of Lin and Falicov. The long axis of the electron pocket makes an angle of 10.6° with the horizontal—this is similar to what was found both theoretically² and experimentally.^{20,25}

Careful inspection of Fig. S3 leads us to believe that this cross section is somewhat “S-shaped”. This observation is corroborated experimentally for arsenic by Priestley, *et al.*²⁵ and by Cooper and Lawson,²⁰ who performed cyclotron resonance experiments for arsenic at 1.15 K. This “S-shape” has also been calculated by Falicov and Lin as being the case for the analogous cross section in antimony.²⁴

The intersection of the binary-bisectrix plane with an electron pocket at L results in the cross section of area 0.096\AA^{-2} presented in Fig. S4, and the intersection of the trigonal-binary plane with an electron pocket at L yields the contour of area 0.026\AA^{-2} displayed in Fig. S5—

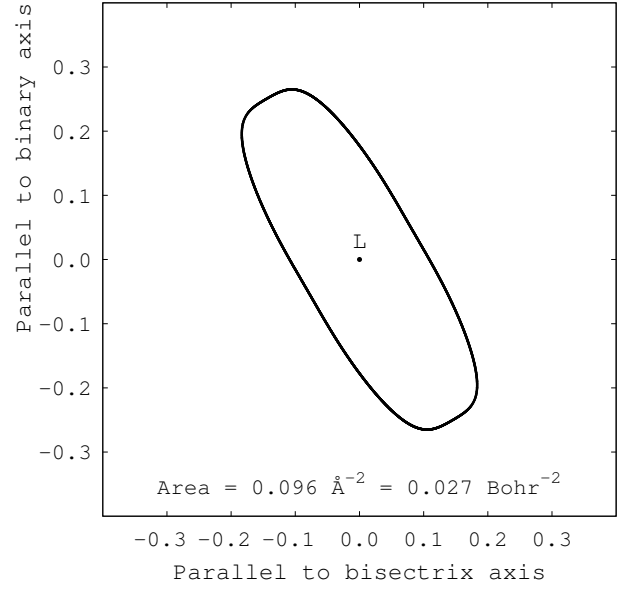


FIG. S4: Electron pocket: binary-bisectrix plane through L. This figure and the resulting area have been obtained using a Fermi energy recomputed from the Wannier-interpolated DOS of A7 arsenic at 0 GPa. All distances are in \AA^{-1} . This contour can be located in the top panel of the middle column of Fig. 6.

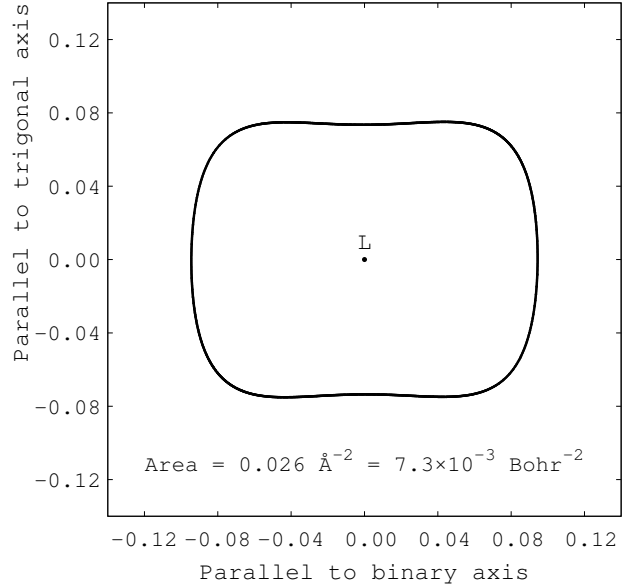


FIG. S5: Electron pocket: trigonal-binary plane through L. This figure and the resulting area have been obtained using a Fermi energy recomputed from the Wannier-interpolated DOS of A7 arsenic at 0 GPa. All distances are in \AA^{-1} .

this cross section corresponds to that obtained by slicing the electron pocket of Fig. S3 in the vertical direction at L. These results, as well as those that follow for the hole Fermi surface of arsenic at 0 GPa, are summarized in Table I, along with data resulting from theory and experiment available in the literature.

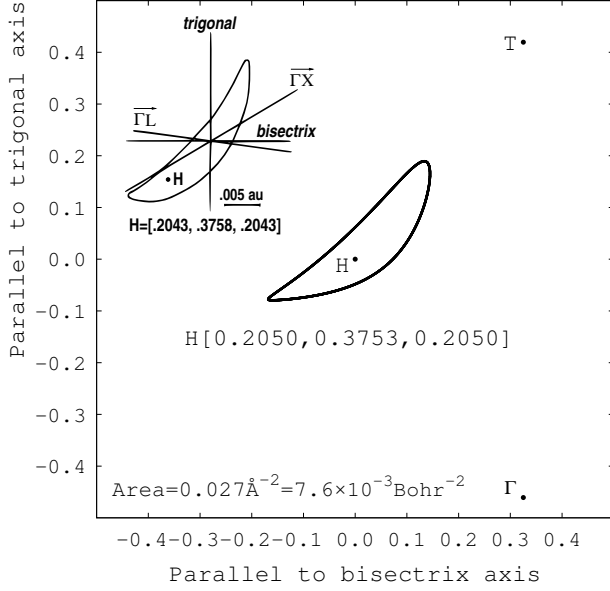


FIG. S6: Hole pocket—one of six lobes of the hole crown: trigonal-bisectrix plane through H. This figure and the resulting area have been obtained using a Fermi energy recomputed from the Wannier-interpolated DOS of A7 arsenic at 0 GPa. All distances are in \AA^{-1} . This contour can be located in the top panel of the left-hand column of Fig. 6. The inset is the analogous cross section as calculated by Lin and Falicov.² The points Γ and T are included as an aid to viewer orientation.

2. Features of the Hole Fermi Surface

The hole Fermi surface of arsenic at 0 GPa is an object centered at T composed of six lobe-like pockets (three up, three down) connected by long thin cylinders or necks. The intersection of the trigonal-bisectrix plane (the mirror plane) with one of the lobe-like hole pockets results in the Fermi contour displayed in Fig. S6. Once again, we include as an inset of this figure the analogous cross section obtained by Lin and Falicov in 1966.² Again, our respective contours are similar, though slightly different toward the extremities. The area of our cross section is 0.027 \AA^{-2} , which is about twice as large as in Ref. 25 (experiment), approximately 1% larger than in Ref. 20 (experiment), and approximately 20% smaller than that obtained by Lin and Falicov (although in Ref. 25 this value of Lin and Falicov is retracted and it is claimed instead that the value is difficult to determine).

The maximum of the fifth band, designated as “H”, occurs in the mirror plane. It is labeled in Fig. S6, along with the points Γ and T, which have been included in the diagram for orientation purposes. Using a 2-D interpolation grid with a density of 5000 \mathbf{k} -points per length of the reciprocal lattice vector, we determine the coordinates of one of these six H points to be $[0.2050, 0.3753, 0.2050]$ (fractional coordinates with respect to the reciprocal lattice vectors). The coordinates for the corresponding H point as found by Lin and Fal-

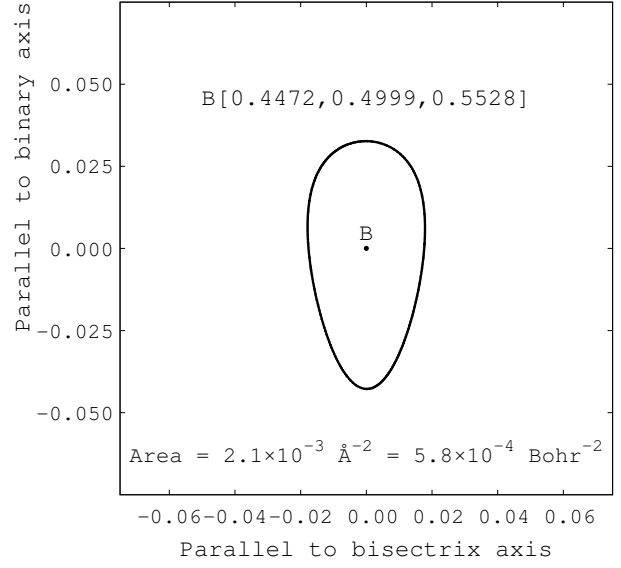


FIG. S7: Hole pocket—one of six necks of the hole crown: binary-bisectrix plane through T. This figure and the resulting area have been obtained using a Fermi energy recomputed from the Wannier-interpolated DOS of A7 arsenic at 0 GPa. All distances are in \AA^{-1} . This contour can be located in the top panel of the middle column of Fig. 6.

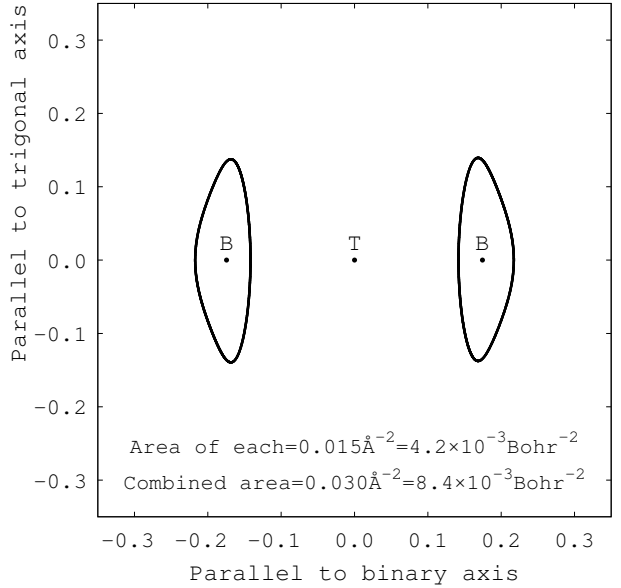


FIG. S8: Hole pocket: trigonal-binary plane through T. This figure and the resulting areas have been obtained using a Fermi energy recomputed from the Wannier-interpolated DOS of A7 arsenic at 0 GPa. All distances are in \AA^{-1} .

icov are $[0.2043, 0.3758, 0.2043]$ and so the agreement is excellent. We use our point H to determine the angle that the lobe makes with the vertical to be 37.8° (this is the angle between HT and ΓT), which agrees closely with experiment.²⁵

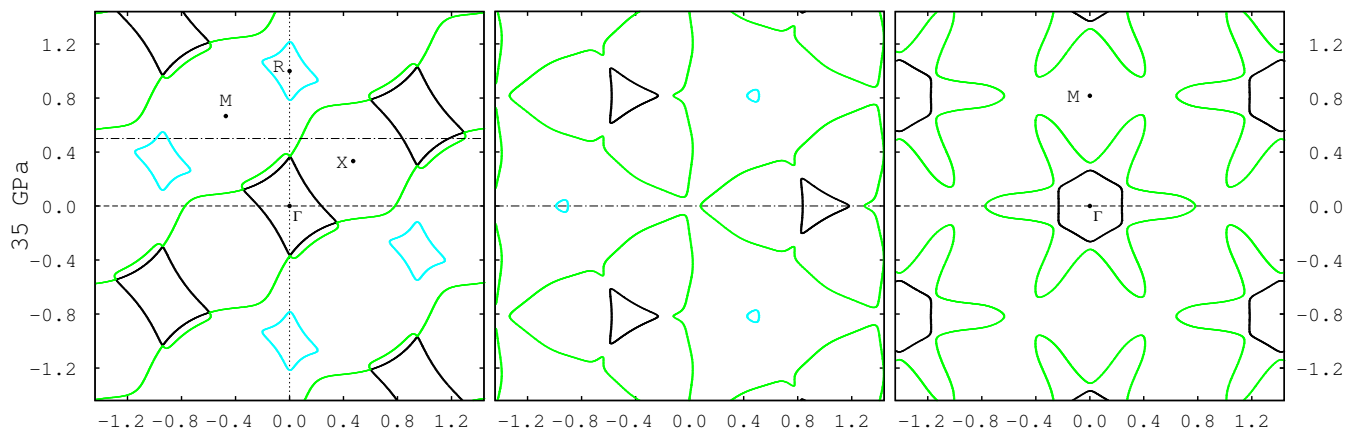


FIG. S9: This figure is the unfolded version of the bottom row of Fig. 6, obtained by slicing up the BZ of the corresponding one-atom primitive cell of sc arsenic at 35 GPa. The orientations of each of the three panels correspond to those of Fig. 6, as do the dotted, dashed and dotted-dashed lines. Distances in this figure are fractional with respect to the length of the reciprocal lattice vector of the corresponding two-atom unit cell. This is so that this figure can be overlaid and compared to the bottom row of Fig. 6. The second, third and fourth bands contribute the black, green and blue contours, respectively. In particular, the second band provides cubic hole pockets at Γ (in the left panel these are seen sliced along the body diagonal) and the fourth band provides cubic electron pockets at the points R.

The intersection of the binary-bisectrix plane through T with the hole Fermi surface yields the contours of the cross sections of the six necks, each located about a point B along a TW line. One such cross section is depicted in Fig. S7. Again using a 2-D interpolation grid with a density of 5000 k -points per length of the reciprocal lattice vector, we determine the fractional coordinates of one of these six B points to be $[0.4472, 0.4999, 0.5528]$. The coordinates for one of the B points as found by Lin and Falicov are $[0.4617, 0.5, 0.5383]$, close to our own results.

Finally, as we did with the electron Fermi surface, we look at the intersection of the trigonal-binary plane passing through Γ with the hole Fermi surface, which is illustrated in Fig. S8. We see that in this orientation, two necks are sliced vertically—they are on opposite sides of T.

Once again, all results obtained for both the electron and hole Fermi surfaces of arsenic at 0 GPa are summarized in Table I, and contrasted against results previously published in the literature. We now proceed to investigate further the evolution of the Fermi surface of arsenic with pressure.

Appendix SIV: Pressure Dependence of the Fermi Surface of Arsenic: A7 \rightarrow SC Transition

1. SC Arsenic Using the One-Atom Primitive Cell

In Fig. S9 we display contours of the Fermi surfaces of sc arsenic at 35 GPa using the one-atom primitive cell. (The self-consistent calculation for the ground state potential of sc arsenic at 35 GPa using the one-atom primitive cell is performed using a $40 \times 40 \times 40$ Monkhorst-Pack grid of k -points.) This figure is the “unfolded” version of the bottom row of Fig. 6, where the calculations have been performed for sc arsenic at 35 GPa using the

two-atom unit cell. The orientation of the panels correspond between the two figures. The contours displayed in Fig. S9 are provided by bands 2 (black), 3 (green) and 4 (blue). The second band provides hole pockets at Γ , and the fourth band provides electron pockets at R. The distances in Fig. S9 are fractional with respect to the length of the reciprocal lattice vector of the two-atom unit cell of sc arsenic—this is so that the folded and unfolded versions of the figure can be overlaid and compared with each other. Points R and M that appear in the left panel of Fig. S9 fold onto the points Γ and X respectively when the two-atom unit cell is used. The origin of the middle panel of the figure is the point $[\frac{1}{4}, \frac{1}{4}, \frac{1}{4}]$, corresponding to the T point in the case of the two-atom unit cell—in order for the middle panel of this figure to correspond to the middle panel of the bottom row of Fig. 6, the plane containing the points T, W and U in the two-atom case is slid downward by the fractional coordinates $[\frac{1}{4}, \frac{1}{4}, \frac{1}{4}]$.

The top panel of Fig. S10 depicts another view of the unfolded Fermi surface of arsenic in the sc phase at 35 GPa. This slice through the one-atom sc BZ contains Γ and the points X, and we can see the cubic hole surface centered on Γ provided by the second band. The green contours are provided by the third band. The fourth band does not cross the Fermi level for any of the k -points on this slice through the sc BZ, hence the fourth band provides no contours to this slice. In order to be consistent, distances once again are with respect to the length of the reciprocal lattice vector of the two-atom unit cell.

In the bottom panel of Fig. S10, the XCRYSDEN package²³ has been used to plot out the three-dimensional Fermi surface corresponding to the view displayed in the top panel of the figure. Surfaces due to bands 2, 3 and 4 are merged to form the object shown. The second band provides the dark green cube centered on Γ . The fourth band provides the dark blue cubes centered on R. The corresponding slice of the BZ for the two-atom represen-

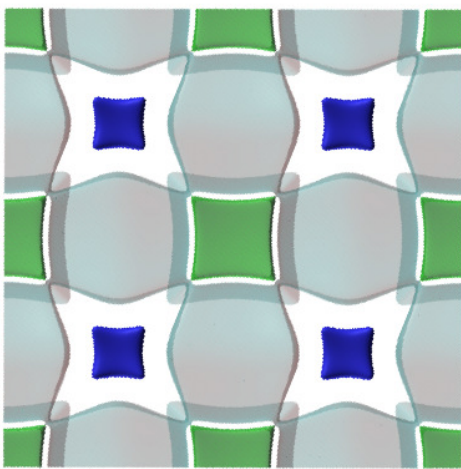
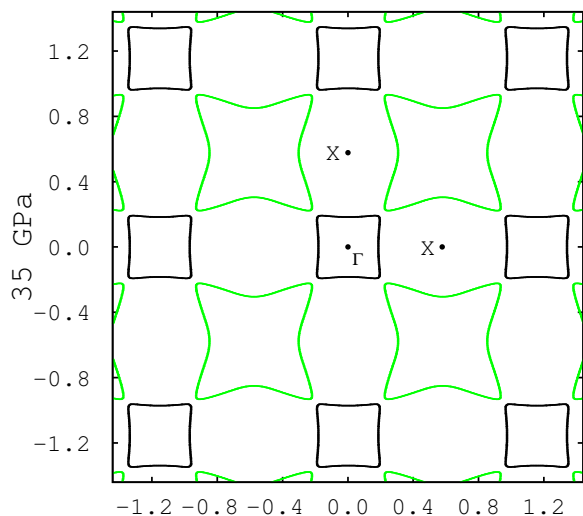


FIG. S10: Another perspective of the Fermi surface of sc arsenic at 35 GPa using the one-atom primitive cell. In the top panel, we see that for this slice through the BZ only the second and third bands provide contours (in black and green, respectively). This perspective allows us to see the actual cubic cross section of the unfolded hole pocket at Γ . Distances in the top panel are once again fractional with respect to the length of the reciprocal lattice vector of the two-atom unit cell. In the bottom panel, the 3-D Fermi surface in the direction corresponding to the slice of the top panel is plotted. The second band provides the dark green cube at Γ , the fourth band provides the dark blue cubes at the points R, and the third band provides the remainder of the object shown.

tation of sc arsenic at 35 GPa is shown in Fig. S11—it is the folded version of the top panel of Fig. S10.

2. Higher-Pressure Transitions of Arsenic

Watching Animations 01–03,^{31–33} we observe that arsenic ceases to be in the sc phase over 53–54 GPa, and enters the bcc phase over 95–96 GPa—there are quite dramatic changes to the Fermi contours taking place at these transition pressures. The pressures at which these tran-

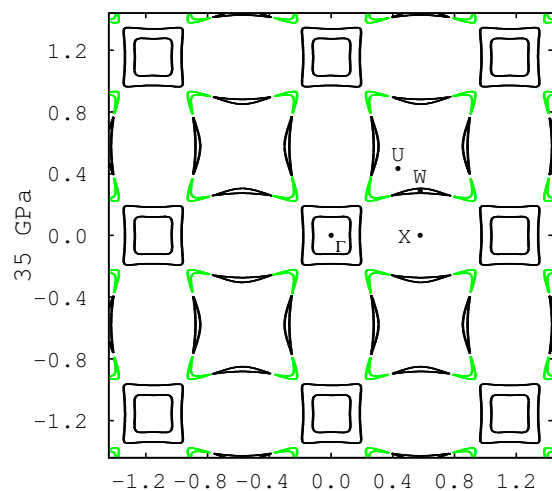


FIG. S11: Simple-cubic arsenic at 35 GPa using the two-atom unit cell: this figure is the folded version of the top panel of Fig. S10.

sitions occur are as expected since this work is based on our earlier findings,¹⁰ as we have already mentioned. Between the sc and bcc phases, arsenic has an incommensurate structure (with increasing pressure, the progression of the phases of arsenic is $A7 \rightarrow sc \rightarrow incomm \rightarrow bcc$ as discussed in Ref. 10). As stated in that work, we do not attempt to model properly the phase existing between sc and bcc—a periodically-repeated two-atom unit cell cannot model an incommensurate structure. We have acknowledged this point by simply labeling as “incomm” the structure we find between the sc and bcc phases. That being stated, in the interest of thoroughness and continuity we nevertheless use our earlier findings for this “incomm” phase (over the range of 54–95 GPa) in the same way as we have done for the other pressures studied.

At 55 GPa, arsenic is in our fictitious “incomm” phase. At 200 GPa, arsenic is in the bcc phase. In Fig. S12 we display for 55 GPa and 200 GPa the left-hand, middle and right-hand columns in the style of Fig. 6: the panels of the left-hand column refer to intersections of the trigonal-bisectrix plane with the BZ, those of the middle column to intersections of the binary-bisectrix plane through T with the BZ, and those of the right-hand column to intersections of the binary-bisectrix plane through Γ with the BZ. Once again, all distances in this figure are fractional with respect to the length of the reciprocal lattice vector. The dotted, dashed and dotted-dashed lines are as described for Fig. 6. In the two-atom representation of the bcc phase of arsenic, the points T, W and U merge. This is evinced by comparing both rows of Fig. S12: in the left-hand panels the points T and U are seen to be merged at 200 GPa, while in the middle panels this is the case for all three points. Only bands 5 (in black) and 6 (in green) are represented in this figure, though at 55 GPa bands 5–8 cross the Fermi level and at 200 GPa it is crossed by bands 3–8. For our

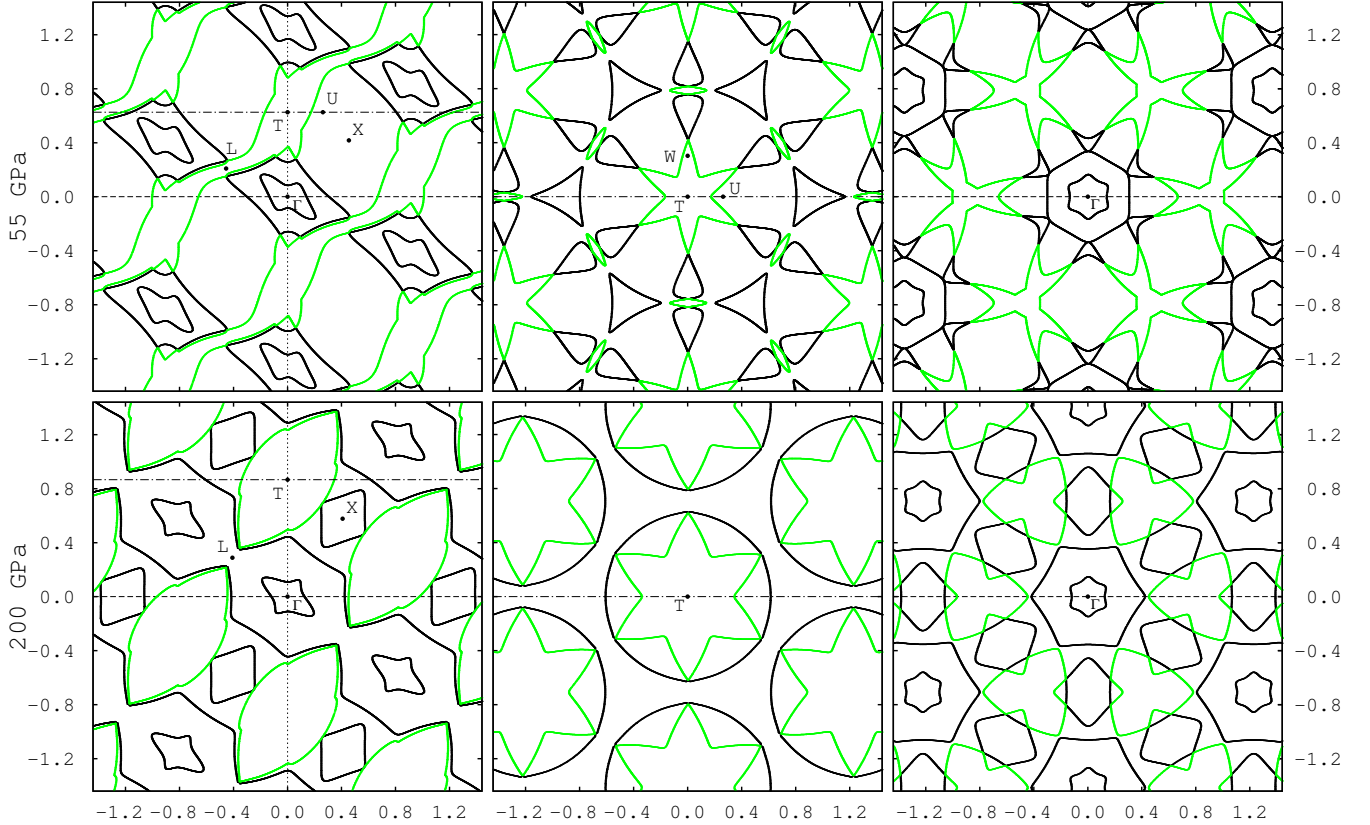


FIG. S12: Pressure dependence of the Fermi surface of arsenic: 55–200GPa. This figure is in the style of Fig. 6. The top row represents slices of the BZ for arsenic at 55 GPa, when it is in our fictitious “incomm” phase. In the bottom row we display the slices for bcc arsenic at 200 GPa.

two-atom periodically-repeated representation of arsenic at 55 GPa, bands 7 and 8 missing from the figure both provide small electron pockets at T. In the 200 GPa case, missing bands 3 and 4 give rise to very small hole pockets at X, while bands 7 and 8 produce electron pockets at T.

In a further elucidation of the might of Wannier interpolation, we conclude this section by inviting the reader to peruse some or all of the remaining animations that accompany this work.^{34–46} Of the 16 animations that have been included, we have been discussing the three which illustrate the evolution of the Fermi surface of arsenic with pressure.^{31–33} For each of the six pressures (0, 10, 20, 35, 55 and 200 GPa) that contribute to Fig. 6 and to Fig. S12, we have plotted the two-dimensional band structure of the fifth and sixth bands corresponding to a sequence of slices through the BZ. We slice the BZ in two different directions producing two animations for each pressure:^{34–45} parallel to the trigonal-bisectrix plane and parallel to the binary-bisectrix plane. In addition to the 2-D band structures, the resulting electron and hole Fermi contours are also plotted.

Lastly, as we have also been working with the one-atom primitive cell of arsenic at 35 GPa, we have created an animation displaying the Fermi contours provided by

bands 2, 3 and 4 resulting again from such slices through the BZ.⁴⁶ The left-hand panel of each frame of this animation displays the contours arising from a slice that is parallel to a plane corresponding to the trigonal-bisectrix plane. The right-hand panel displays the contours resulting from slices parallel to a plane corresponding to the binary-bisectrix plane in the two-atom case.

Appendix SV: Wannier-Interpolated Densities of States of A7, SC and BCC Arsenic

Finally we inspect the evolution of the DOS of arsenic in the immediate vicinity of the A7 \rightarrow sc transition, and present our results in Fig. S13. This figure consists of a series of six panels that are ordered from top to bottom, starting with the left-hand column. The top left panel displays the DOS of arsenic at 29 GPa, when it is in the sc phase. In the panels that follow, we see successive superpositions of the DOSs that result as the pressure is decreased at intervals of 1 GPa. In the bottom right panel, the six DOSs from 29 to 24 GPa are shown. Changes in the DOS through the sc \rightarrow A7 transition as the pressure is decreased are more clearly seen in this direction than in the reverse. We observe a marked change in the DOS

between 26 and 27 GPa, as evinced by the sharp wiggles that first appear in the top right panel of the figure. These emerging van Hove singularities indicate the onset of the Peierls-type cubic to rhombohedral distortion. We reported in Ref. 10 that in the GGA-PBE case the A7 \rightarrow sc transition occurs at 28 ± 1 GPa, coinciding with the pressure at which the atomic positional parameter z reaches its high-symmetry value of $1/4$. The signature we notice in the top right panel of Fig. S13 however seems to coincide with the change in the cell angle α (we showed in Ref. 10 that α reaches its high-symmetry value at a lower pressure than does z). In other words, the electronic change occurring as the pressure is increased appears to be driving α to 60° . Yet arsenic cannot be said

to be in the sc phase until both α and z have reached their high-symmetry values. As reported in Ref. 10, for GGA-PBE the difference between these two pressures is approximately 2 GPa. The above observation does coincide however with what we see in the animations that accompany this work.^{31–33} As we discussed in Sec. V, a folding of the Fermi surfaces is seen to occur by 27 GPa.

It is useful to be able to compare DOS plots with the band structures to which they correspond. We offer in Fig. S14 just such a comparison for the A7, sc and bcc phases of arsenic at 0, 35 and 200 GPa, respectively. In each case, the Fermi level is indicated by the solid red line. As the pressure is increased, the lowest bands begin to appear free-electron-like.

-
- ¹ O. Degtyareva, M. I. McMahon, and R. J. Nelmes, High Pressure Res. **24**, 319 (2004).
- ² P. J. Lin and L. M. Falicov, Phys. Rev. **142**, 441 (1966).
- ³ J. R. Yates, X. Wang, D. Vanderbilt, and I. Souza, Phys. Rev. B **75**, 195121 (2007).
- ⁴ X. Wang, J. R. Yates, I. Souza, and D. Vanderbilt, Phys. Rev. B **74**, 195118 (2006).
- ⁵ X. Wang, D. Vanderbilt, J. R. Yates, and I. Souza, Phys. Rev. B **76**, 195109 (2007).
- ⁶ F. Giustino, J. R. Yates, I. Souza, M. L. Cohen, and S. G. Louie, Phys. Rev. Lett. **98**, 047005 (2007).
- ⁷ N. Marzari and D. Vanderbilt, Phys. Rev. B **56**, 12847 (1997).
- ⁸ I. Souza, N. Marzari, and D. Vanderbilt, Phys. Rev. B **65**, 035109 (2001).
- ⁹ N. Marzari, A. A. Mostofi, J. R. Yates, I. Souza, and D. Vanderbilt (2012), arXiv:1112.5411v2.
- ¹⁰ P. Silas, J. R. Yates, and P. D. Haynes, Phys. Rev. B **78**, 174101 (2008).
- ¹¹ H. J. Beister, K. Strössner, and K. Syassen, Phys. Rev. B **41**, 5535 (1990).
- ¹² T. Kikegawa and H. Iwasaki, J. Phys. Soc. Jpn. **56**, 3417 (1987).
- ¹³ See the Supplemental Material of Ref. 10, available at <http://link.aps.org/supplemental/10.1103/PhysRevB.78.174101>, for the convergence properties of the A7 \rightarrow sc phase transition.
- ¹⁴ G. H. Wannier, Phys. Rev. **52**, 191 (1937).
- ¹⁵ N. Marzari, D. Vanderbilt, A. De Vita, and M. C. Payne, Phys. Rev. Lett. **82**, 3296 (1999).
- ¹⁶ See the Supplemental Material of Ref. 47, available at <http://link.aps.org/supplemental/10.1103/PhysRevB.88.134103>, for the following: a review of the BZ of the two-atom primitive cell of A7 arsenic; a discussion concerning the choice of the number of Wannier functions to construct in order to set up an “exact tight-binding” model of the system at each given pressure, from which Wannier interpolations can be performed; an elaboration on the features of the electron and hole Fermi surfaces of A7 arsenic at 0 GPa; an investigation of sc arsenic at 35 GPa using the one-atom primitive cell to inspect the “unfolded” Fermi surfaces, and to compare with the folded ones resulting from the use of the two-atom unit cell; results of our studies of arsenic at pressures beyond which it is no longer in the sc phase (once again using the two-atom unit cell); an elaboration on our studies of the DOS of arsenic as it undergoes the A7 \rightarrow sc phase transition, and DOSs and corresponding band structures for A7, sc, and body-centered-cubic (bcc) arsenic; and various animations created to illustrate the evolution of the Fermi surface of arsenic across the A7 \rightarrow sc transition.
- ¹⁷ P. Giannozzi, S. Baroni, N. Bonini, M. Calandra, R. Car, C. Cavazzoni, D. Ceresoli, G. L. Chiarotti, M. Cococcioni, I. Dabo, et al., J. Phys.: Condens. Matter **21**, 395502 (2009), <http://dx.doi.org/10.1088/0953-8984/21/39/395502>.
- ¹⁸ A. A. Mostofi, J. R. Yates, Y.-S. Lee, I. Souza, D. Vanderbilt, and N. Marzari, Comput. Phys. Commun. **178**, 685 (2008), <http://www.wannier.org>.
- ¹⁹ J. P. Perdew, K. Burke, and M. Ernzerhof, Phys. Rev. Lett. **77**, 3865 (1996).
- ²⁰ G. S. Cooper and A. W. Lawson, Phys. Rev. B **4**, 3261 (1971).
- ²¹ M. H. Cohen, Phys. Rev. **121**, 387 (1961).
- ²² L. M. Falicov and S. Golin, Phys. Rev. **137**, A871 (1965).
- ²³ A. Kokalj, Comput. Mater. Sci. **28**, 155 (2003).
- ²⁴ L. M. Falicov and P. J. Lin, Phys. Rev. **141**, 562 (1966).
- ²⁵ M. G. Priestley, L. R. Windmiller, J. B. Ketterson, and Y. Eckstein, Phys. Rev. **154**, 671 (1967).
- ²⁶ L. R. Windmiller, Phys. Rev. **149**, 472 (1966).
- ²⁷ C. S. Ih and D. N. Langenberg, Phys. Rev. B **1**, 1425 (1970).
- ²⁸ M. H. Cohen, L. M. Falicov, and S. Golin, IBM J. Res. Dev. **8**, 215 (1964).
- ²⁹ R. M. Martin, *Electronic Structure: Basic theory and practical methods* (Cambridge University Press, 2004).
- ³⁰ L. F. Mattheiss, D. R. Hamann, and W. Weber, Phys. Rev. B **34**, 2190 (1986).
- ³¹ *Animation-01-Trigonal-bisectrix-plane-through-Gamma-with-pressure.gif*.
- ³² *Animation-02-Binary-bisectrix-plane-through-T-with-pressure.gif*.
- ³³ *Animation-03-Binary-bisectrix-plane-through-Gamma-with-pressure.gif*.
- ³⁴ *Animation-04-0GPa-parallel-to-trigonal-bisectrix-plane.gif*.
- ³⁵ *Animation-05-0GPa-parallel-to-binary-bisectrix-plane.gif*.
- ³⁶ *Animation-06-10GPa-parallel-to-trigonal-bisectrix-*

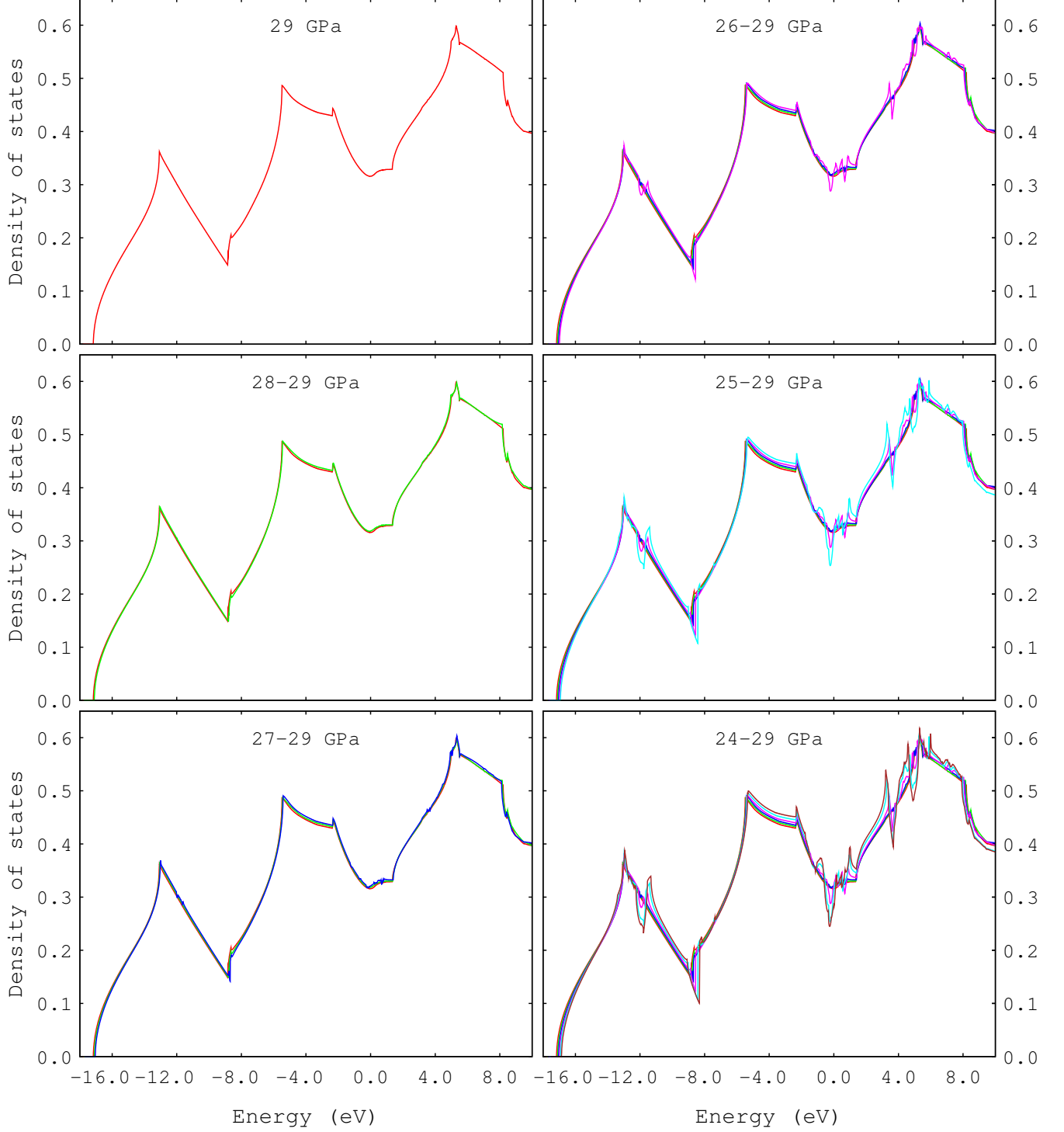


FIG. S13: Evolution of the DOS of arsenic across the $sc \rightarrow A7$ phase transition. The DOSs are referenced to the Fermi level. The panels are ordered from top to bottom starting with the left-hand column. The DOS of sc arsenic at 29 GPa is presented in the top left panel. DOSs at 1 GPa intervals and with decreasing pressure are added to each successive image in the panels that follow. A marked change occurs between 26 and 27 GPa, as can be seen in the top right panel. The emerging van Hove singularities indicate the onset of the Peierls-type cubic to rhombohedral distortion. This agrees with the pressure at which the folding of the Fermi surfaces is seen to occur, as discussed in Sec. V and which can be observed by viewing the relevant animations.^{31–33} In Ref. 10 we reported that the electronic change that occurs across the transition drives the atomic positional parameter z to its high-symmetry value—our results here suggest instead that it is the rhombohedral angle α that is being driven to its high-symmetry value.

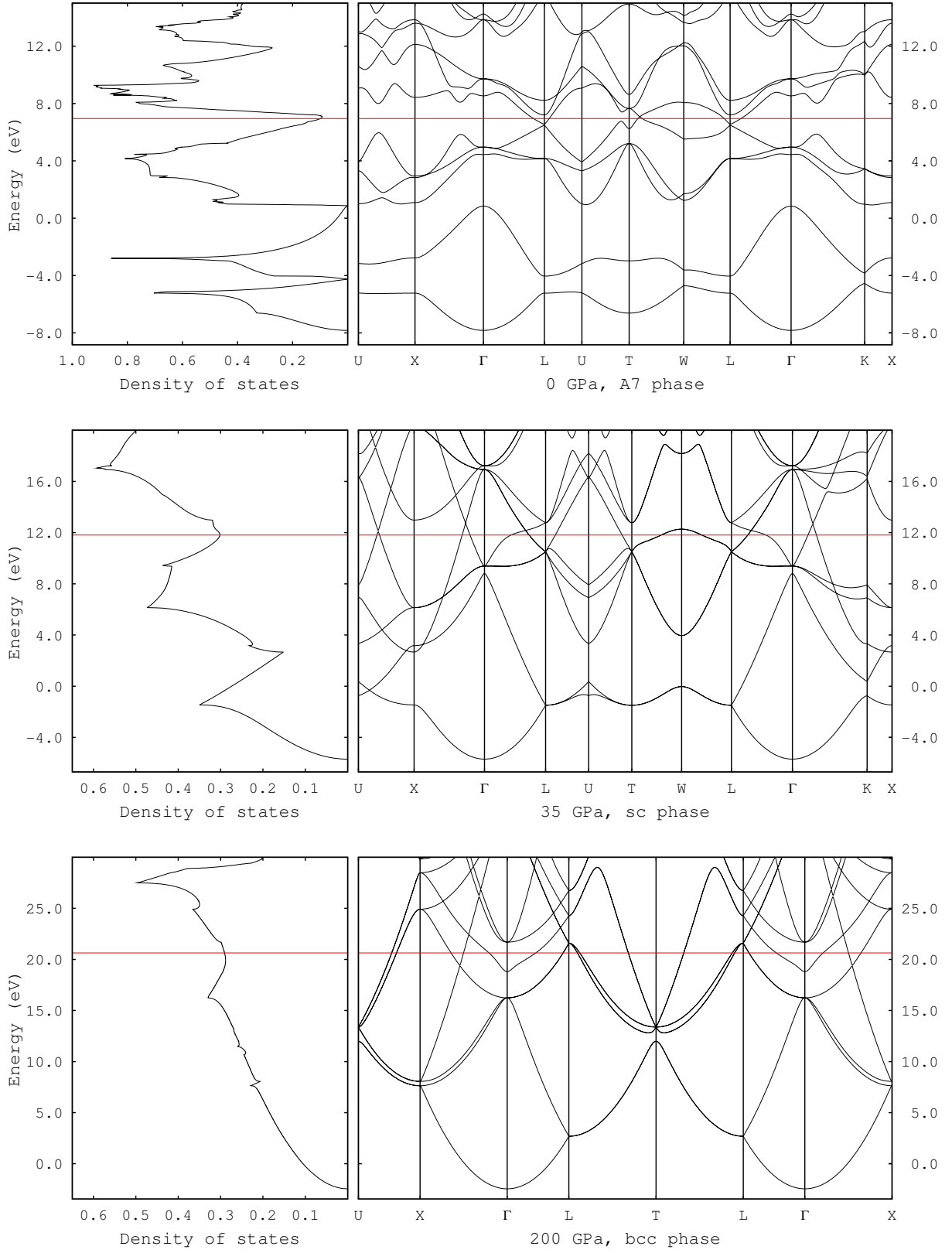


FIG. S14: The Wannier-interpolated DOSs of A7, sc and bcc arsenic and corresponding band structures. In each case, the Fermi level is indicated by the solid red line. At 0 GPa, arsenic is a semimetal—from the band structure in the top panel we see that the fifth band provides tiny hole pockets at a point (called B) close to T along the TW line. The sixth band provides electron pockets at L. At 35 GPa, arsenic is a metal—the band structure displayed for sc arsenic in the middle panel is “folded”—it results from performing our calculations on a unit cell containing two atoms. Scanning the band structures from top to bottom, it can be seen that low-lying bands appear free-electron-like with increasing pressure.

- plane.gif.*
- ³⁷ *Animation-07-10GPa-parallel-to-binary-bisectrix-plane.gif.*
- ³⁸ *Animation-08-20GPa-parallel-to-trigonal-bisectrix-plane.gif.*
- ³⁹ *Animation-09-20GPa-parallel-to-binary-bisectrix-plane.gif.*
- ⁴⁰ *Animation-10-35GPa-parallel-to-trigonal-bisectrix-plane.gif.*
- ⁴¹ *Animation-11-35GPa-parallel-to-binary-bisectrix-plane.gif.*
- ⁴² *Animation-12-55GPa-parallel-to-trigonal-bisectrix-plane.gif.*
- ⁴³ *Animation-13-55GPa-parallel-to-binary-bisectrix-plane.gif.*
- ⁴⁴ *Animation-14-200GPa-parallel-to-trigonal-bisectrix-plane.gif.*
- ⁴⁵ *Animation-15-200GPa-parallel-to-binary-bisectrix-*

- plane.gif.*
- ⁴⁶ *Animation-16-35GPa-primitive-cell-showing-both-directions-simultaneously.gif.*
- ⁴⁷ P. K. Silas, P. D. Haynes, and J. R. Yates, Phys. Rev. B **88**, 134103 (2013).
- ⁴⁸ Thus far, our Fermi energies have been obtained using the PWSCF code.¹⁷ Unless otherwise indicated, our depictions of the Fermi surface of arsenic have also been obtained using these values. Our measurements of the cross sections of the Fermi surface of arsenic at 0 GPa however have been calculated using a more precise value of the Fermi energy, recomputed from a Wannier-interpolated DOS we present in Sec. SV.
- ⁴⁹ References in which the numbering is not preceded by an “S” refer to Figures, Sections or Tables that appear in the accompanying paper (Ref. 47).